Commun. Theor. Phys. **77** (2025) 055201 (8pp)
https://doi.org/10.1088/1572-9494/ad9c46
CSTR: 32041.14.CTP.ad9c46

Color dipole cross-section from unifying the color-dipole picture and improved saturation models

G R Boroun

Department of Physics, Razi University, Kermanshah 67149, Iran

E-mail: boroun@razi.ac.ir

Received 29 August 2024, revised 20 November 2024
Accepted for publication 5 December 2024
Published 12 February 2025

Abstract

We present an analysis of the color-dipole picture for determination of the gluon density at low-x which is obtained from the Altarelli-Martinelli equation by expansion at distinct points of expansion. The dipole cross-sections with respect to the improved saturation model of Bartels–Golec-Biernat–Kowalski are obtained in a wide range of transverse sizes r and compared with the Golec-Biernat-W ü sthoff model. We find that the model gives a good description of the dipole cross-section at large r which confirms saturation and matches the perturbative QCD result at a small r due to the significant role of the running of the gluon distribution.

Keywords: color dipole model, saturation, gluon density, low-x

1. Introduction

One of the remaining challenges in particle and nuclear physics at low x in future colliders is understanding the structure of hadrons in terms of gluons. These novel opportunities will be opened at new-generation facilities, such as the large hadron electron collider (LHeC) [1], the Future Circular hadron-electron Colliders (FCC-he) [2] and the Electron-Ion Collider (EIC) [3]. The electron–proton center-of-mass energies in the LHeC and FCC-he are proposed to be $\sqrt{s} = 1.3$ TeV and $\sqrt{s} = 3.5$ TeV respectively. The kinematics of the LHeC in the (x, Q^2) plane in neutral currents reaches $\simeq$1 TeV^2 and $\simeq 10^{-6}$ for Q^2 and x respectively [1, 4]. The center-of-mass energies in electron-ion colliders (i.e., EIC and EIcC) are 15–20 GeV for EIcC and 30–140 GeV for EIC [3].

Gluons, which mediate the strong interaction, contain essential information about the hadron and play a crucial role in the properties of those. The gluon distribution in deep inelastic scattering (DIS) has been studied by authors in [5–10]. The gluon density is dominant at low x (where $x \cong \frac{Q^2}{W^2} \ll 1$ and W denotes the virtual-photon-proton center-of-mass energy) and this determination could be a test of perturbative QCD (pQCD) or a probe of new effects. One of the interesting models is the color-dipole model (CDM), which was first proposed by the authors in [11, 12, 13] and then extended in [14–22]. This model is represented by the hadronic fluctuations (in terms of the $q\bar{q}$) that interact in a gauge-invariant manner as color-dipole states with the proton via two-gluon exchange. In CDM, the gluon saturation effects are important at low scales. Indeed, the growth of the gluon density is tamed, which is related to unitarity. This result from gluon recombination was defined in terms of the nonlinear evolution equations [23, 24, 25]. A further refinement of the saturation was proposed by the Balitsky–Kovchegov (BK) [26, 27, 28] equation. In this model, the dipole scattering amplitude was proposed in terms of the Wilson operators.

The dipole cross-section is directly connected via a Fourier transform to the unintegrated gluon distribution (UGD) at small x, whose evolution in x is regulated by the Balitsky–Fadin–Kuraev–Lipatov (BFKL) equation [29–31]. The BFKL equation governs the evolution of the UGD, where the k_t-factorization is used in the high-energy limit in which the QCD interaction is described in terms of the quantity which depends on the transverse momentum of the gluon (i.e., k_t^2) [32]. Interpretation of the high-energy interactions predicts that the small x gluons in a hadron wave function should form a Color Glass Condensate [33–35] which describes the over-populated gluonic state.

Dipole representation provides a convenient description of DIS at small x, where the dipole cross-section of the scattering between the virtual photon γ^* and the proton is

Table 1. The coefficients are summarized with respect to Fits 0–2 in [36].

Fit	m_l	m_c	m_b	σ_0[mb]	λ	$x_0/10^{-4}$	C	μ_0^2[GeV^2]	A_g	λ_g
0	0.14	—	—	23.58 ± 0.28	0.270 ± 0.003	2.24 ± 0.16	—	—	—	—
1	0.14	1.4	—	27.32 ± 0.35	0.248 ± 0.002	0.42 ± 0.04	—	—	—	—
2	0.14	1.4	4.6	27.43 ± 0.35	0.248 ± 0.002	0.40 ± 0.04	—	—	—	—
1	0	1.3	—	22.60 ± 0.26	—	—	0.29 ± 0.05	1.85 ± 0.20	1.18 ± 0.15	0.11 ± 0.03
2	0	1.3	4.6	22.93 ± 0.27	—	—	0.27 ± 0.04	1.74 ± 0.16	1.07 ± 0.13	0.11 ± 0.03

related to the imaginary part of the $(q\bar{q})p$ forward scattering amplitude. The dipole cross-section in the Golec-Biernat and W ü sthoff (GBW) [12, 13, 36] model is a good description of the DIS data with only three fitted parameters (i.e.,σ_0, x_0 and λ), and takes the following form

$$\sigma_{\rm dip}(x, \boldsymbol{r}) = \sigma_0\{1 - \exp(-r^2 Q_s^2(x)/4)\}, \tag{1}$$

where $Q_s(x)$ plays the role of the saturation momentum, parametrized as $Q_s^2(x) = Q_0^2(x_0/x)^\lambda$ (with $Q_0^2 = 1\,\text{GeV}^2$) and r is the transverse dipole size of the $q\bar{q}$ pair. The dipole cross-section saturates to a constant value at large r, $\sigma_{\rm dip} \simeq \sigma_0$, and vanishes for small r which makes the color transparency, $\sigma_{\rm dip} \sim r^2$, which is a purely pQCD phenomenon. As is well known, this model is reasonable only at small transverse momenta k_t (after the Fourier transform), as its exponential decay contradicts the expected perturbative behavior at large k_t. The Bartels–Golec-Biernat–Kowalski (BGK) model [37, 38], is another phenomenological approach to dipole cross-section and reads

$$\sigma_{\rm dip}(x, \boldsymbol{r}) = \sigma_0\left\{1 - \exp\left(\frac{-\pi^2 r^2 \alpha_s(\mu_r^2) xg(x, \mu_r^2)}{3\sigma_0}\right)\right\}. \tag{2}$$

The evolution scale μ_r^2 is connected to the size of the dipole by $\mu_r^2 = \frac{C}{r^2} + \mu_0^2$ and $xg(x, \mu_r^2)(\equiv G(x, \mu_r^2))$ is the gluon distribution function. The parameters C and μ_0 are determined [36] from the fits to the HERA data and obtained owing to the dipole quark mass. The Bjorken variable x is also modified, since the photon wave function depends on the mass of the quark in the $q\bar{q}$ dipole, by the following form

$$x \to \bar{x}_f = x\left(1 + \frac{4m_f^2}{\mu_r^2}\right) = \frac{\mu_r^2 + 4m_f^2}{\mu_r^2 + W^2}, \tag{3}$$

Therefore the coefficients are defined [36] according to the quark masses $m_f = 0.14$, 1.4 and 4.6 GeV (for light, charm and bottom respectively) in table 1.

In small dipole size, $\sigma_{\rm dip}(x, \boldsymbol{r})$ (i.e., equation (2)) is proportional to the gluon distribution from the DGLAP evolution as

$$\sigma_{\rm dip}(x, \boldsymbol{r}) \simeq \frac{\pi^2 r^2}{3} \alpha_s(C/r^2) xg(x, C/r^2), \tag{4}$$

and has the property of color transparency. For large dipole size, equation (2) in the limit $\mu_r^2 \simeq \mu_0^2$ reads

$$\sigma_{\rm dip}(x, \boldsymbol{r}) \simeq \sigma_0\left\{1 - \exp\left(\frac{-\pi^2 r^2 \alpha_s(\mu_0^2) xg(x, \mu_0^2)}{3\sigma_0}\right)\right\}, \tag{5}$$

where in this limit, the saturation scale[1] of the GBW model is proportional to the gluon distribution at the scale μ_0^2 by the following form

$$Q_s^2(x) = \frac{4\pi^2}{3\sigma_0} \alpha_s(\mu_0^2) xg(x, \mu_0^2), \tag{6}$$

where the gluon distribution at the initial condition is defined by $xg(x, \mu_0^2) = A_g x^{-\lambda_g}(1 - x)^{5.6}$. The gluon distribution in the BGK model is usually [36–39] evolved with the DGLAP equations truncated to the gluonic sector and parametrized at the initial scale of μ_0^2. In section II we present the gluon distribution from the color-dipole picture (CDP). In section III we present the comparison of the model results with the GBW model. Finally, we summarize our findings in Conclusions.

2. The gluon distribution from the color-dipole picture

In QCD, structure functions are defined as convolution of universal parton momentum distributions inside the proton and coefficient functions, which contain information about the boson-parton interaction. The longitudinal structure function is directly related to the singlet and gluon distributions in the proton [40], and defined as a convolution integral over $F_2(x, Q^2)$ and the gluon distribution $xg(x, Q^2)$ by an effect of order $\alpha_s(Q^2)$ as

$$F_L(x, Q^2) = C_{\rm L,ns+s}(\alpha_s(Q^2), x) \otimes F_2(x, Q^2) + \langle e^2 \rangle C_{\rm L,g}(\alpha_s(Q^2), x) \otimes xg(x, Q^2), \tag{7}$$

where $\langle e^2 \rangle = n_f^{-1} \sum_{i=1}^{n_f} e_i^2$ and the symbol $\otimes$denotes convolution according to the usual prescription. The standard collinear factorization formula for the longitudinal structure function at low x reads

$$F_L(x, Q^2) = \langle e^2 \rangle C_{\rm L,g}(\alpha_s(Q^2), x) \otimes xg(x, Q^2), \tag{8}$$

[1] Namely, for dipole cross-sections depending on DGLAP evolved gluon PDF the saturation scale is obtained by numerically solving the implicit equation for the critical line. This is explicitly done for the BGK model in the original reference (see equation (22) of the Bartels–Biernat–Kowalski′s paper or the discussion in section V of the Kowalski-Teaney′s paper of [37, 38]).

where the gluonic coefficient function $C_{\mathrm{L,g}}$ can be written in a perturbative expansion as follows [41]

$$C_{\mathrm{L,g}}(\alpha_s(Q^2), x) = \sum_{n=0}\left(\frac{\alpha_s}{4\pi}\right)^{n+1} c_{L,g}^{(n)}(x), \tag{9}$$

where n denotes the order in running coupling.

Using the expansion method [42] for the gluon distribution function at an arbitrary point $z = a$ as

$$G\left(\frac{x}{1-z}\right)|_{z=a} = G\left(\frac{x}{1-a}\right) + \frac{x}{1-a}(z-a) \times \frac{\partial G(\frac{x}{1-a})}{\partial x} + O(z-a)^2, \tag{10}$$

where the series

$$\frac{x}{1-z}\Big|_{z=a} = \frac{x}{1-a}\sum_{k=1}^{\infty}\left[1 + \frac{(z-a)^k}{(1-a)^k}\right] \tag{11}$$

is convergent for $|z-a| < 1$. After doing the integration and retaining terms only up to the first derivative in the expansion, we have

$$F_L(x, Q^2) = \langle e^2\rangle A(x, Q^2) G\left(\frac{x}{1-a}\left(1 - a + \frac{B(x, Q^2)}{A(x, Q^2)}\right)\right) = \langle e^2\rangle A(x, Q^2) G(x_g, Q^2), \tag{12}$$

where $x_g = kx$, $k = \frac{1}{1-a}(1 - a + \frac{B}{A})$ and 'a' has an arbitrary value $0 \leqslant a < 1$ [43–46]. In equation (12) the kernels A and B read

$$A(x, Q^2) = \int_0^{1-x} \frac{1}{1-z} C_{\mathrm{L,g}}(\alpha_s, 1-z)\mathrm{d}z, \tag{13}$$

and

$$B(x, Q^2) = \int_0^{1-x} \frac{z-a}{1-z} C_{\mathrm{L,g}}(\alpha_s, 1-z)\mathrm{d}z. \tag{14}$$

At the leading-order (LO) approximation, equation (12) can be rewritten as

$$F_L(x, Q^2) = \frac{10\alpha_s}{27\pi} G\left(\frac{x}{1-a}\left(\frac{3}{2} - a\right)\right). \tag{15}$$

This result reproduced the longitudinal structure function determined by the authors in [47, 48] if we expand the gluon distribution around the point $a = 0.666$ as

$$F_L(x, Q^2) = \frac{10\alpha_s}{27\pi} G(2.5x, Q^2) (=\text{Ref.}[32]). \tag{16}$$

For a wide range of different expanding points, the gluon distribution is defined into the longitudinal structure function by the following form[2]

$$G(x, Q^2) = \frac{3\pi}{\alpha_s(Q^2)\sum_i e_i^2} F_L(k_L x, Q^2), \tag{17}$$

where

$$k_L = \frac{2(1-a)}{3-2a}. \tag{18}$$

In terms of the photoabsorption cross-section, $\sigma_{\gamma_L^* p}$, the longitudinal structure function is given by

$$F_L\left(W^2\left(=\frac{Q^2}{x}\right), Q^2\right) = \frac{Q^2}{4\pi^2\alpha}\sigma_{\gamma_L^* p}\left(W^2\left(=\frac{Q^2}{x}\right), Q^2\right), \tag{19}$$

where $\sigma_{\gamma_L^* p}(W^2, Q^2)$ is derived from an ansatz [11, 14, 15, 16, 18, 19, 20] for the W-dependent dipole cross-section by the following form[3]

$$\sigma_{\gamma_L^* p}(W^2, Q^2) = \frac{\alpha R_{e^+e^-}}{3\pi}\sigma^{(\infty)}(W^2) I_L(\eta, \mu) G_L(u) = \frac{\sigma_{\gamma p}(W^2)}{\lim\limits_{\eta\to\mu(W^2)} I_T\left(\frac{\eta}{\rho}, \frac{\mu(W^2)}{\rho}\right) G_T(u)} I_L(\eta, \mu) G_L(u), \tag{20}$$

where $R_{e^+e^-} = 3\sum_i e_i^2$ and $\sigma^{(\infty)}(W^2)$, which stems from the normalization of the $q\bar{q}$-dipole proton cross-section, is replaced owing to the smooth transition to $Q^2 = 0$ photoproduction [21]. The quantity $I_L(\eta, \mu)$ is given by

$$I_L(\eta, \mu) = \frac{\eta - \mu}{\eta} \times \left(1 - \frac{\eta}{\sqrt{1 + 4(\eta - \mu)}} \times \ln\frac{\eta(1 + \sqrt{1 + 4(\eta - \mu)})}{4\mu - 1 - 3\eta + \sqrt{(1 + 4(\eta - \mu))((1 + \eta)^2 - 4\mu)}}\right), \tag{21}$$

where

$$\eta \equiv \eta(W^2, Q^2) = \frac{Q^2 + m_0^2}{\Lambda_{\mathrm{sat}}^2(W^2)}, \tag{22}$$

and

$$\mu \equiv \mu(W^2) = \eta(W^2, Q^2 = 0) = \frac{m_0^2}{\Lambda_{\mathrm{sat}}^2(W^2)}, \tag{23}$$

with the saturation scale $\Lambda_{\mathrm{sat}}^2(W^2)$,

$$\Lambda_{\mathrm{sat}}^2(W^2) = C_1\left(\frac{W^2}{1\mathrm{GeV}^2}\right)^{C_2}, \tag{24}$$

and constant parameters, based on [21], read

$$m_0^2 = 0.15\ \mathrm{GeV}^2,\ C_1 = 0.31\ \mathrm{GeV}^2;\quad C_2 = 0.29. \tag{25}$$

The dipole cross-section $\sigma^{(\infty)}(W^2)$, in equation (20), is evaluated from the photoproduction cross-section as [19, 20]

$$\sigma^{(\infty)}(W^2) = \frac{3\pi}{\alpha R_{e^+e^-}}\frac{\sigma(W^2)}{\ln\frac{\rho}{\mu}}, \tag{26}$$

[2] When $n_f = 4$, equation (17) can be reduced to equation (15), as it corresponds to transform a fixed flavor number into variable flavor number.

[3] The model of [18] is based on off-diagonal generalized vector dominance (GVDM) and some simple ansatz for the behavior of the dipole cross-section in both very large and small color-dipole sizes.

where

$$\sigma(W^2) = 0.003056\left(34.71 + \frac{0.3894\pi}{M^2}\ln^2\frac{W^2}{(M_p+M)^2}\right) + 0.0128\left(\frac{(M_p+M)^2}{W^2}\right)^{0.462} \tag{27}$$

with $\sigma(W^2)$ is given in unit of mb, and $M = 2.15$ GeV, M_P is proton mass in unit of GeV. The parameter ρ is related to the longitudinal-to-transverse ratio of the photoabsorption cross-sections by the constant value $\frac{4}{3}$ owing to [19, 20–22]. In the photoproduction limit (i.e., $Q^2 = 0$), where $\eta \to \mu(W^2)$, $G_T(u \equiv \frac{\xi}{\eta}) \simeq 1$. The parameter ξ[4] is fixed at $\xi = \xi_0 = 130$ and therefore

$$\lim_{\eta\to\mu(W^2)} I_T^{(1)}\left(\frac{\eta}{\rho}, \frac{\mu(W^2)}{\rho}\right) = \ln\frac{\rho}{\mu(W^2)}. \tag{28}$$

The function $G_L(u)$ is given by

$$G_L(u) = \frac{2u^3+6u^2}{2(1+u)^3} \simeq \begin{cases} 3\left(\frac{\xi}{\eta}\right)^2 & (\eta \gg \xi), \\ 1 - 3\left(\frac{\eta}{\xi}\right)^2 & (\eta \ll \xi), \end{cases} \tag{29}$$

In conclusion, in the scale μ_r^2, the gluon distribution in the color-dipole picture is defined by the following form

$$G(x,\mu_r^2) = \frac{9\mu_r^2}{4\pi\alpha\alpha_s(\mu_r^2)R_{e^+e^-}}\frac{\sigma(W^{2*})}{\ln\frac{\rho}{\mu^*}} I_L(\eta^*,\mu^*)G_L(u^*), \tag{30}$$

where $W^{2*} = k_L^{-1}W_r^2 = k_L^{-1}(\mu_r^2/x)$, $\eta^* = (\mu_r^2 + m_0^2)/\Lambda_{\rm sat}^2(W^{2*})$ and $\mu^* = m_0^2/\Lambda_{\rm sat}^2(W^{2*})$. The effective dipole cross-section is evaluated according to the following form

$$\sigma_{\rm dip}(x,\boldsymbol{r}) = \sigma_0\left\{1 - \exp\left(-\frac{3\pi(C+\mu_0^2r^2)}{4\sigma_0\alpha R_{e^+e^-}}\frac{\sigma(W^{2*})}{\ln\frac{\rho}{\mu^*}} \times I_L(\eta^*,\mu^*)G_L(u^*)\right)\right\} \tag{31}$$

as a function of r and the expansion point a in different values of x, which also depends on the quark effective mass. The relation of the CDP gluon density in a proton to the dipole cross-section in the BGK model will be calculated in the next section.

3. Numerical results

The results for the gluon distribution function (i.e., equation (30)) in the CDM are presented based on the expansion point $z = a$ over a wide range of x and $\mu^2 = Q^2$ in Figures 1–2. The gluon distribution functions, with and without the rescaling variable (i.e., equation (3), $x \to x(1 + 4m_c^2/\mu^2)$) including the charm quark mass, are defined at $Q^2 = 10$ and 100 GeV^2. In figure 1, for $Q^2 = 10$ and 100 GeV^2, the gluon distribution with the rescaling variable at the expanding points $a = 0.9$ (solid curve, black) and $a = 0$ (dot curve, blue) and without the rescaling variable at the expanding points $a = 0.9$ (dashed curve, red) and $a = 0$ (dashed-dot curve, green) are compared with the CJ15LO [49] along with total errors (bands, cyan). In this figure, we observe that the gluon distribution at the expansion point $a = 0.9$ (with and without the rescaling variable) is comparable with the CJ15LO at $Q^2 = 10$ GeV^2 and at the expansion point $a = 0$ (with and without the rescaling variable) is comparable with the CJ15LO at $Q^2 = 100$ GeV^2 within the uncertainties errors across a wide range of x. In figure 2, the same results as in figure 1 are presented for the gluon distribution compared with the NNPDF3.0LO [50] along with total errors across a wide range of x. We observe that the results at low Q^2 values are comparable with parametrization

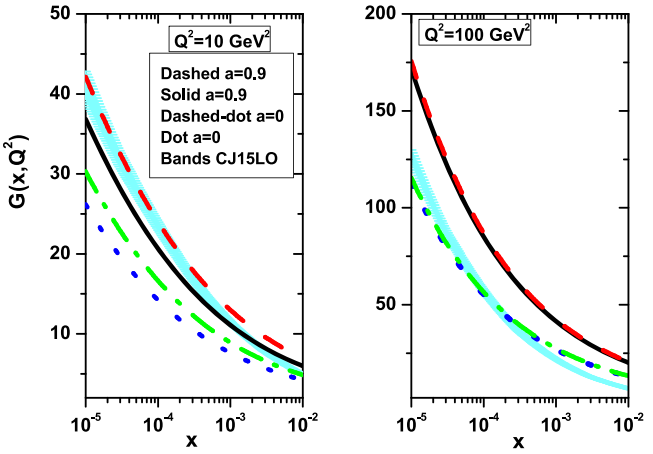

Figure 1. The gluon distribution function $G(x, Q^2)$ with the rescaling variable at the expanding points $a = 0.9$ (solid curve, black) and $a = 0$ (dot curve, blue) and without the rescaling variable at the expanding points $a = 0.9$ (dashed curve, red) and $a = 0$ (dashed-dot curve, green) compared with the CJ15LO [49] as accompanied with total errors (bands, cyan).

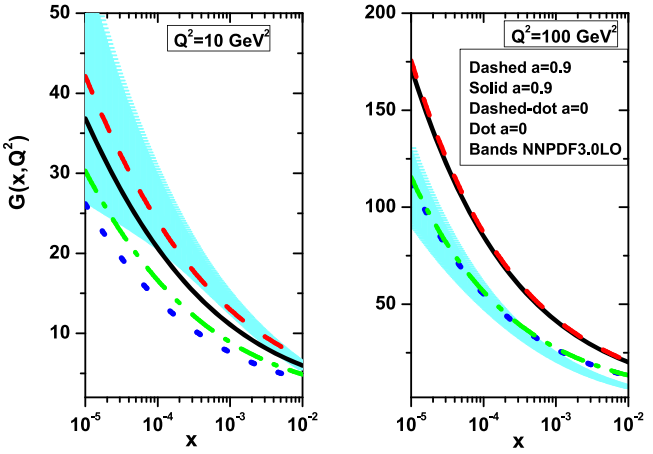

Figure 2. The same as figure 1 compared with the NNPDF3.0LO [50].

[4] The constant parameter ξ restricts the masses of the contributing mass $q\bar{q}$ states via

$$M_{qq}^2 \leqslant m_{\rm i}^2(W^2) = \xi\Lambda_{\rm sat}^2(W^2).$$

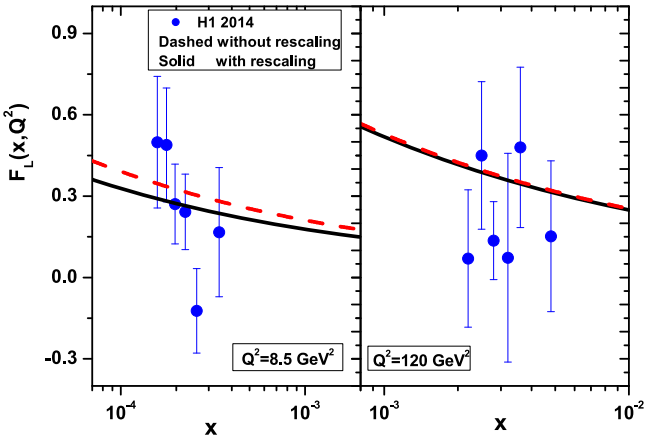

Figure 3. The longitudinal structure function $F_L(x, Q^2)$ with (solid curves) and without (dashed curves) the rescaling variable plotted at fixed Q^2 (left: $Q^2 = 8.5$ GeV^2, right: $Q^2 = 120$ GeV^2) as a function of x variable, compared with the H1 Collaboration data [51]. Experimental data (circles, H1 2014) are from the H1 Collaboration [51] as accompanied with total errors.

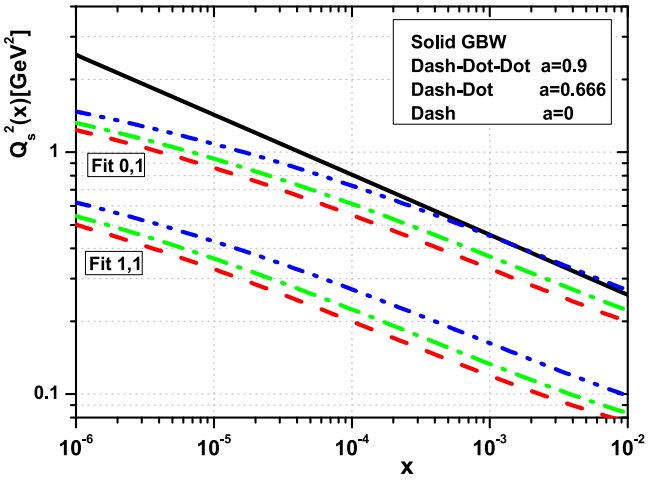

Figure 4. The saturation scale at the scale μ_0^2 in the CDP model with the expansion points (a = 0, 0.666 and 0.9) with the parameters from the fits in table 1 compared with the GBW model (solid line) with the charm contribution.

groups as the expansion point increases, and at large Q^2 values, they are comparable at lower expansion points.

According to the results[5] at low and high Q^2 values in figures 1 and 2, the longitudinal structure functions are obtained at fixed Q^2 values (i.e., $Q^2 = 8.5$ and 120 GeV^2) and compared with the results of the H1 Collaboration [51] as a function of x. The longitudinal structure function extracted with and without the rescaling variable at Q^2 values are in good agreement with experimental data compared to those in [51], with total errors shown in figure 3.

The saturation scale with the x and a dependencies from the color-dipole models at the scale μ_0^2 is given by

$$Q_s^2(x,\, a) = \frac{3\pi\mu_0^2}{\alpha\sigma_0 R_{e^+e^-}} \frac{\sigma(W_0^{2*})}{\ln\frac{\rho}{\mu_0^*}} I_L(\eta_0^*,\, \mu_0^*) G_L(u_0^*), \qquad (32)$$

where this saturation scale connects the GBW form of the dipole cross-section with the CDP. In figure 4, we compare the saturation scales from the expansion points with the GBW model with charm from the Fits in table 1, as the coefficients σ_0, λ and x_0 are read from the first three rows of table 1 and the coefficients C and μ_0^2 are read in the next two rows.[6] We observe that the results with increases in the expansion point are close to the GBW model from Fits 0,1 in table 1. As a result, at $x = 10^{-6}$ the saturation scale is order by $\mathrm{GBW}|_{Q_s^2 \approx 2-3\ \mathrm{GeV}^2} >$ Fit 0, 1 $|_{Q_s^2 \approx 1-2\ \mathrm{GeV}^2}$ and at $10^{-4} < x < 10^{-2}$ the results are equal.

In figure 5, we show the ratio of dipole cross-sections $(\sigma_{\mathrm{dip}}/\sigma_0)$ in accordance with the active flavor numbers and the quark mass effects. Quark mass effects are taken as zero for a massive quark i when $\mu^2 < m_i^2$ and the quark treated as fully active when $\mu^2 > m_i^2$. The ratio of dipole cross-sections is obtained, in figure 4, by solving equation (31) using the CDP $xg(x,\, \mu_r^2)$ at the expansion points and compared with the GBW model with the heavy quark contributions. The results are shown for the selected dipole transverse size owing to the Fits 0–2. We observe that our results are sensitive to the expansion point when we compared with the GBW model with the heavy quarks contributions. The indicated values of r in figure 5 are in accordance with the heavy flavors of fit results in table 1. It is clear that for large values of r the two functions are very close, and they differ in the small r region where the running of the gluon distribution and its expansion starts to play a significant role. As a result, the DGLAP improved model with the gluon distribution in the CDP model can be extending to large values of Q^2 (small dipole sizes).

In figure 6, we have calculated the r dependence, at low x ($x = 10^{-3}$ and $x = 10^{-6}$), of the ratio $\sigma_{\mathrm{dip}}(x,\, r)/\sigma_0$ (i.e., equation (31)) owing to the expansion method. Results of calculations with Fits 1, 1 and 2, 2 (in table 1) and comparison with the GBW model with the charm and bottom contributions are presented in figure 6. We see in the left and right plots of figure 6 that for large values of r ($r \gtrsim 1$ fm) the two model results overlap while the CDP results lie below the GBW curves for the interval $0.04\ \mathrm{fm} \lesssim r \lesssim 1$ fm. The deviation of the CDP results from the GBW model in the left and right plots of figure 6 are visible for $r \gtrsim 0.04$ fm, which is due to the running of the gluon distribution, is very visible (especially at very low x). Expanding of the gluon distribution around high and low values of $z = a$ is close to the GBW results in the regions $0.04\ \mathrm{fm} \lesssim r \lesssim 1$ fm and $r \lesssim 0.04$ fm respectively. The uncertainties, in the left and right plots of figure 6, are due to the statistical errors in table 1 in the expansion point $a = 0.666$.

The form of the CDP results for the dipole cross-section $\sigma_{\mathrm{dip}}(x,\, r)$ (i.e., equation (31)) at the expansion points ($a = 0$, 0.666 and 0.9) is shown in figure 7 for $x = 10^{-6}$ and 10^{-2} with the parameters Fit 1, 1 in table 1. In figure 7, a

[5] The gluon density at low and high Q^2 values, with the high and low values of the expansion points, is comparable to the parametrization models (such as CJ15LO and NNPDF3.0LO) respectively.

[6] In fact, changes in gluon distribution cause changes in the parameters. It is good to obtain the parameters by fitting the experimental data with their improved dipole cross-section.

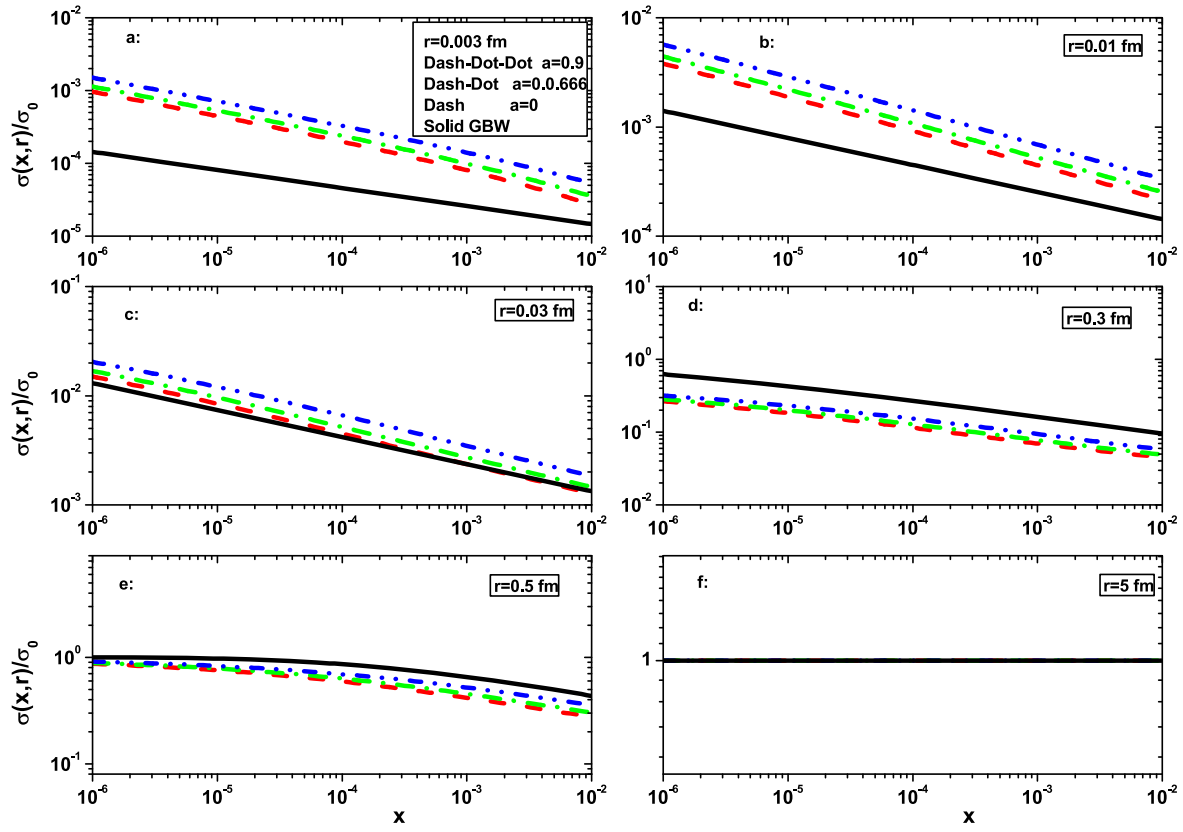

Figure 5. Comparison of the $\sigma_{\rm dip}(x, r)/\sigma_0$ obtained by solving equation (31) using the CDP $xg(x, \mu_r^2)$ at the expansion points with the GBW (solid curves) between thresholds. (a) $r = 0.003$ fm, Fit 2, 2. (b) $r = 0.01$ fm, Fit 2, 2. (c) $r = 0.03$ fm, Fit 1, 1. (d) $r = 0.3$ fm, Fit 1, 1. (e) $r = 0.5$ fm, Fit 0, 1. (c) $r = 5$ fm, Fit 0, 1.

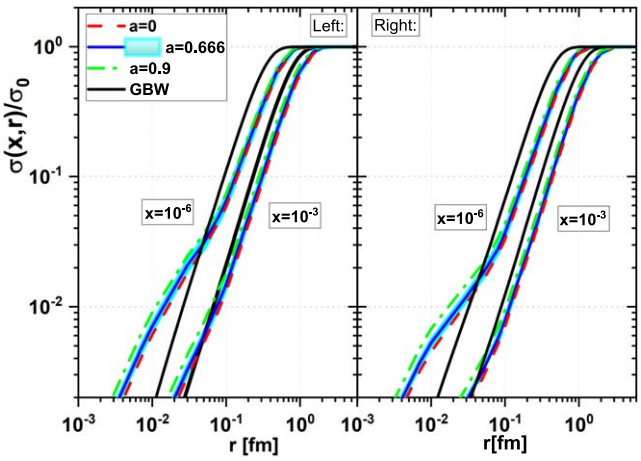

Figure 6. The ratio $\sigma_{\rm dip}(x, r)/\sigma_0$ according to the expansion points for $x = 10^{-6}$ and 10^{-3} with the parameters compared with the GBW model: Left: Fit 1,1. Right: Fit 2,2. The uncertainties in the expansion point $a = 0.666$ are due to the statistical errors in table 1.

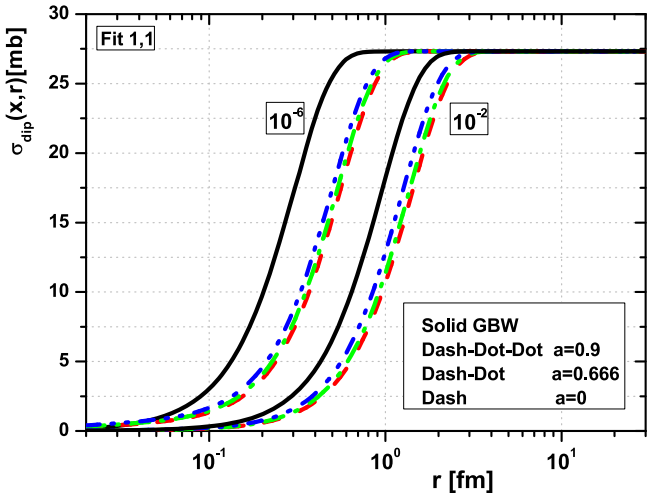

Figure 7. The dipole cross-section $\sigma_{\rm dip}(x, r)$ as a function of transverse dipole size r according to the expansion points for $x = 10^{-6}$ and 10^{-2} with the parameters Fit 1, 1 compared with the GBW model with charm contribution.

comparison with the GBW model (with charm contribution) is done in a wide range of the dipole size r. The CDP results also show that the dipole cross-section features color transparency (i.e., $\sigma_{\rm dip} \sim r^2$) at small r which is perturbative QCD phenomenon and for large r, saturation occurs (i.e., $\sigma_{\rm dip} \simeq \sigma_0$) [52, 53]. We see that the transition between two regimes occurs by decreasing transverse sizes with a decrease of x and this is visible in the large expansion points.

4. Conclusions

In summary, we have used an expansion method of the gluon density in the color-dipole formalism with heavy quark contributions and obtain the dipole cross-section in a wide range of the transverse dipole size r. The gluon density is obtained

at an arbitrary point of expansion of $G(\frac{x}{1-z})|_{z=a}$, where it is dependent on the photoabsorption cross-section in the CDP. The associated CDP gluon density is valid for large as well as small r. The saturation line in the CDP model is dependent on the running of the gluon density on the (x, Q^2)-plane and changed than the GBW model at very low x.

The dipole cross-sections in the improved saturation model are compared with the GBW model owing to the gluon density of the CDP model. The dipole cross-section is modified at small r than the GBW model by the gluon density with the Altarelli-Martinelli equation which is due to the pQCD phenomenon. The transition between the saturation and color transparency regions is dependent on the r, x and the expansion point in our model. We can see that this transition moves towards lower r as x decreases and the expansion point increases.

In conclusion, the color-dipole cross-section from unifying the color-dipole picture and improved saturation models gives a behavior in accordance to the pQCD result with respect to the expansion method.

Acknowledgments

The author is grateful to Razi University for the financial support of this project. I would like to thank D Schildknecht and M Kuroda for helpful comments and discussions.

References

[1] (LHeC Collaboration) *et al* 2021 The large hadron-electron collider at the HL-LHC *J. Phys.* G **48** 110501
[2] (FCC Collaboration) *et al* 2019 FCC physics opportunities: future circular collider conceptual design report volume 1 *Eur. Phys. J.* C **79** 474
[3] Abdul Khalek R *et al* 2022 Science requirements and detector concepts for the electron-ion collider: EIC yellow report *Nucl. Phys.* A **1026** 122447
[4] Klein M 2024 Future deep inelastic scattering with the LHeC arXiv:1802.04317
[5] Chakrabarti D *et al* 2023 Gluon distributions in the proton in a light-front spectator model *Phys. Rev.* D **108** 014009
[6] Bacchetta A, Celiberto F G, Radici M and Taels P 2020 Transverse-momentum-dependent gluon distribution functions in a spectator model *Eur. Phys. J.* C **80** 733
[7] Celiberto F G 2024 High-energy QCD dynamics from bottom flavor fragmentation at the Hi-Lumi LHC *Eur. Phys. J.* C **84** 384
[8] Celiberto F G 2022 A journey into the proton structure: progresses and challenges *Universe* **8** 661
[9] Lipatov A V, Lykasov G I and Malyshev M A 2024 Self-consistent description of HERA data at low Q^2 and soft hadron production at LHC *Phys. Lett.* B **848** 138390
[10] Lu Z and Ma B-Q 2016 Gluon Sivers function in a light-cone spectator model *Phys. Rev.* D **94** 094022
[11] Nikolaev N and Zakharov B G 1991 Colour transparency and scaling properties of nuclear shadowing in deep inelastic scattering *Z. Phys.* C **49** 607
[12] Golec-Biernat K and Wusthoff M 1998 Saturation effects in deep inelastic scattering at low Q^2 and its implications on diffraction *Phys. Rev.* D **59** 014017
[13] Golec-Biernat K and Wusthoff M 1999 Saturation in diffractive deep inelastic scattering *Phys. Rev.* D **60** 114023
[14] Cvetic G, Schildknecht D and Shoshi A 2000 Deep inelastic scattering, QCD, and generalized vector dominance *Eur. Phys. J.* C **13** 301
[15] Schildknecht D 2001 Deep inelastic scattering at low x: Generalized vector dominance and the color dipole picture *Nucl. Phys.* B **99** 121
[16] Schildknecht D, Surrow B and Tentyukov M 2001 Low x scaling in $\gamma^* p$ total cross-section *Phys. Lett.* B **499** 116
[17] Jeong Y S, Kim C S, Luu M V and Reno M H 2014 Color dipole cross section and inelastic structure function *J. High Eergy Phys.* JHEP11(2014)025
[18] Cvetic G, Schildknecht D, Surrow B and Tentyukov M 2001 The Generalized vector dominance color dipole picture of deep inelastic scattering at low x *Eur. Phys. J.* C **20** 77
[19] Kuroda M and Schildknecht D 2016 The color dipole picture of low-x DIS: model-independent and model-dependent results *Phys. Rev.* D **85** 094001
[20] Kuroda M and Schildknecht D 2016 Color dipole picture of deep inelastic scattering, revisited *Int. J. Mod. Phys.* A **31** 1650157
[21] Boroun G R, Kuroda M and Schildknecht D The proton gluon distribution from the color dipole picture arXiv:2206.05672
[22] Schildknecht D 2021 Color-dipole picture versus hard pomeron in deep inelastic scattering *Phys. Rev.* D **104** 014009
[23] Gribov L V, Levin E M and Ryskin M G 1981 Singlet structure function at small x: unitarization of gluon ladders *Nucl. Phys.* B **188** 555
[24] Gribov L V, Levin E M and Ryskin M G 1983 Semihard processes in QCD *Phys. Rept.* **100** 1
[25] Mueller A H and Qiu J-w 1986 Gluon recombination and shadowing at small values of x *Nucl. Phys.* B **268** 427
[26] Balitsky I 1996 Operator expansion for high-energy scattering *Nucl. Phys.* B **463** 99
[27] Kovchegov Y V 1999 Small x F_2 structure function of a nucleus including multiple pomeron exchanges *Phys. Rev.* D **60** 034008
[28] Kovchegov Y V 2000 Unitarization of the BFKL pomeron on a nucleus *Phys. Rev.* D **61** 074018
[29] Fadin V S, Kuraev E A and Lipatov L N 1975 On the pomeranchuk singularity in asymptotically free theories *Phys. Lett.* B **60** 50
[30] Lipatov L N 1976 Reggeization of the Vector Meson and the Vacuum Singularity in Nonabelian Gauge Theories *Sov. J. Nucl. Phys.* **23** 338–45
[31] Balitsky I I and Lipatov L N 1978 The Pomeranchuk Singularity in Quantum Chromodynamics *Sov. J. Nucl. Phys.* **28** 822–9
[32] Kutak K and Stasto A M 2005 Unintegrated gluon distribution from modified BK equation *Eur. Phys. J.* C **41** 343
[33] Iancu E, Leonidov A and McLerran L 2001 Nonlinear gluon evolution in the color glass condensate *Nucl. Phys.* A **692** 583
[34] Iancu E, Leonidov A and McLerran L 2001 The Renormalization group equation for the color glass condensate *Phys. Lett.* B **510** 133
[35] Iancu E, Itakura K and Munier S 2004 Saturation and BFKL dynamics in the HERA data at small x *Phys. Lett.* B **590** 199
[36] Golec-Biernat K and Sapeta S 2018 Saturation model of DIS: an update *J. High Energy Phys.* JHEP03(2018)102
[37] Bartels J, Golec-Biernat K and Kowalski H 2002 A modification of the saturation model: DGLAP evolution *Phys. Rev.* D **66** 014001

[38] Kowalski H and Teaney D 2003 An Impact parameter dipole saturation model *Phys. Rev.* D **68** 114005

[39] Luszczak A, Luszczak M and Schafer W 2022 Unintegrated gluon distributions from the color dipole cross section in the BGK saturation model *Phys. Lett.* B **835** 137582

[40] Altarelli G and Martinelli G 1978 Transverse momentum of jets in electroproduction from quantum chromodynamics *Phys. Lett.* B **76** 89

[41] Moch S, Vermaseren J A M and Vogt A 2005 The longitudinal structure function at the third order *Phys. Lett.* B **606** 123

[42] Gay Ducati M B and Goncalves P B 1997 Analysis of low x gluon density from the F_2 scaling violations *Phys. Lett.* B **390** 401

[43] Boroun G R and Rezaei B 2012 Analysis of the proton longitudinal structure function from the gluon distribution function *Eur. Phys. J.* C **72** 2221

[44] Boroun G R and Rezaei B 2022 Higher order approximations to the longitudinal structure function F_L from the parametrization of F_2 based on the Laplace transformation *Phys. Rev.* D **105** 034002

[45] Boroun G R and Rezaei B 2021 An evaluation of the proton structure functions F_2 and F_L at small x *Phys. Letts.* B **816** 136274

[46] Boroun G R 2018 Longitudinal structure function from logarithmic slopes of F_2 at low x *Phys. Rev.* C **97** 015206

[47] Cooper-Sarkar A M *et al* 1988 Measurement of the longitudinal structure function and the small x gluon density of the proton *Z. Phys.* C **39** 281

[48] Cooper-Sarkar A M and Devenish R C E 2003 The Rise and fall of F_2 at low x *Acta. Phys. Polon.* B **34** 2911–28

[49] Owens J F, Accardi A and Melnitchouk W 2013 Global parton distributions with nuclear and finite-Q^2 corrections *Phys. Rev.* D **87** 094012

[50] (NNPDF Collaboration) *et al* 2015 Parton distributions for the LHC Run II *J. High Energy Phys.* JHEP04(2015)040

[51] Andreev V *et al* (H1 Collaboration) 2014 Measurement of inclusive ep cross sections at high Q^2 at $\sqrt{s} = 225$ and 252 GeV and of the longitudinal proton structure function F_L at HERA *Eur. Phys. J.* C **74** 2814

[52] Golec-Biernat K 2002 Saturation and geometric scaling in DIS at small x *J. Phys.* G **28** 1057

[53] Golec-Biernat K 2002 Saturation effects in DIS at low x *Acta. Phys. Polon.* B **33** 2771–90